

Rapid Electrohydrodynamic Lithography Using Low-Viscosity Polymers

Pola Goldberg-Oppenheimer and Ullrich Steiner*

This study explores a number of low-viscosity glass-forming polymers for their suitability as high-speed materials in electrohydrodynamic (EHD) lithography. The use of low-viscosity polymer films significantly reduces the patterning time (to below 10 s) compared to earlier approaches, without compromising the high fidelity of the replicated structures. The rapid pace of this process requires a method to monitor the completion of EHD pattern formation. To this end, the leakage current across the device is monitored and the sigmoidal shape of the current curve is correlated with the various stages of EHD pattern formation.

Keywords:

- capacitors
- electrohydrodynamic lithography
- pattern formation
- polymers
- viscosity

1. Introduction

Electrohydrodynamic lithography (EHL) is a lithographic method that makes use of the destabilization of a polymer film by means of an electric field.^[1–3] While the origin of the underlying electrohydrodynamic (EHD) surface instabilities has long been known,^[4–6] its use for high-performance lithography is relatively recent, and provides a way to replicate 100-nm-sized patterns in a simple and straightforward fashion. The benefit of EHL pattern replication is the possibility of contactless lithography^[7] along with the electric field coupling to smaller self-assembled morphologies within the film,^[8] thus providing a means for hierarchical structure control spanning many length scales. The setup of a typical EHL experiment is shown in Figure 1.

One of the limiting factors has, however, been the slow replication dynamics. Typical polymeric resists require many minutes or hours for the pattern replication to complete, as shown, for example, by Leach et al.^[9] This problem is intrinsic to EHL, caused by the interplay of two factors:

- 1) Most resists consist of high-molecular-weight polymers that have a high melt viscosity in their accessible temperature range. Since the electric field strength is limited by the

dielectric strength of the materials in the narrow capacitor gap in Figure 1, the obtainable strain rates are generally low. Reducing the molecular weight of the polymers often reduces the polymer glass transition temperature, thus precluding the requirement for solidification above room temperature. Consequently, glass-forming materials are required, which form a low-viscosity liquid in the accessible temperature window.

- 2) The arrest of pattern formation during a narrow, well-defined time window is essential. While too short an exposure to the electric field results in incomplete pattern replication, too long annealing times give rise to coalescence of small-scale structures, which degrades pattern fidelity. This is exacerbated by the fact that the direct observation of submicrometer patterns in a capacitor slit is nearly impossible and that optical quality control is not scalable.

Herein, our purpose is to introduce an EHL system that combines these two requirements. We investigate a number of commonly available low-viscosity materials, and reduce the completion of EHL to a few seconds. Low-viscosity epoxy materials were also studied by Dickey et al., who reported similarly low patterning times.^[10] An essential requirement for short-time EHL patterning is the precise termination of the pattern formation process. While Dickey and co-workers achieve this by crosslinking of the sample, we introduce a method for the online surveillance of the EHL process during this short time span by monitoring the current across the capacitor gap. Since the current is passed through the leaky dielectric once it spans the capacitor gap, the overall capacitor current is a good measure for EHL completion.

[*] Prof. U. Steiner, P. Goldberg-Oppenheimer
Cavendish Laboratory
Department of Physics
University of Cambridge
J. J. Thomson Avenue, Cambridge CB3 0HE (UK)
E-mail: u.steiner@phy.cam.ac.uk

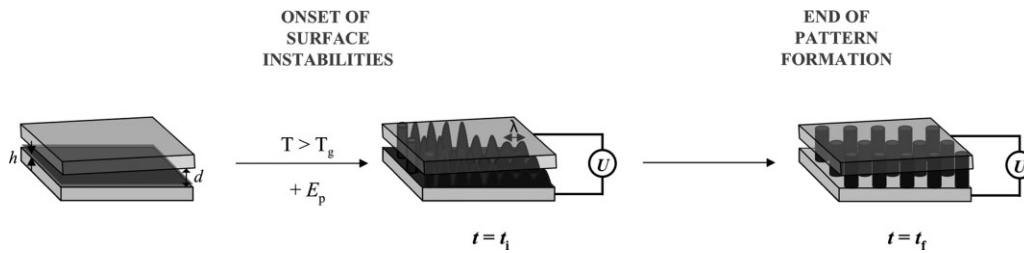


Figure 1. Schematic representation of the experimental setup. The thin film in the capacitor is liquefied by raising the temperature above the glass transition temperature (T_g) of the resist. The amplification of a capillary surface instability is triggered by applying a voltage U . With time the instability causes the formation of liquid bridges between the two plates. The kinetics of pattern formation is observed by either optical microscopy through a transparent electrode or by monitoring the current flowing in the circuit. The time t_i corresponds to the time when the first column spans the two plates, while t_f is the time when the column formation process is completed. The wedge geometry of the device is greatly exaggerated in the drawing. E_p = electric field in the polymer film.

2. Stability Analysis

The physical principles underlying the destabilization of thin films by electric fields are well understood.^[2,3,11–15] Here, we briefly summarize the model describing the early-stage kinetics of pattern formation (linear stability analysis). The experimental configuration is schematically shown in Figure 1. A thin resist layer on one electrode is opposed by the second, thus leaving an air gap. An applied potential difference U across the two electrodes gives rise to an electric field across the dielectric material and air gap. The dielectric discontinuity at the film/air interface in the capacitor gives rise to the formation of displacement charges which couple to the electric field, causing a destabilizing electrostatic pressure p_{el} :

$$p_{el} = -\varepsilon_0 \varepsilon_p (\varepsilon_p - 1) E_p^2 = -\varepsilon_0 \varepsilon_p (\varepsilon_p - 1) \frac{U^2}{[\varepsilon_p d - (\varepsilon_p - 1)h]^2} \quad (1)$$

where E_p is the electric field in the polymer film, ε_0 is the dielectric permittivity of the vacuum, ε_p is the dielectric constant of the polymer, h is the local film thickness, and d is the capacitor plate spacing. While a perfectly homogeneous film is stable, a lateral pressure variation induces in-plane flow. In the lubrication approximation,^[16] assuming zero slip at the substrate and no lateral stresses at the film surface:

$$\frac{\partial h}{\partial t} = \frac{\partial}{\partial x} \left[\frac{h}{3\eta} \frac{\partial p}{\partial x} \right] \quad (2)$$

where t is the time, x a lateral coordinate, and η the viscosity. $p = p_{el} + p_L$ is the total interfacial pressure consisting of the destabilizing electrostatic pressure and the stabilizing Laplace pressure, $p_L = -\gamma(\partial^2 h / \partial x^2)$, with the surface tension γ . p couples to the omnipresent capillary waves of the liquid surface, which destabilizes part of the mode spectrum. This is described by the well-established linear stability analysis, where a sinusoidal ansatz:

$$h(q, t) = h_0 + \xi \exp\left(iqx + \frac{t}{\tau}\right) \quad (3)$$

is used with Equation (2). τ is a characteristic constant for the temporal evolution of mode q , ξ is the wave amplitude, and h_0 is the averaged film thickness. In the long-wavelength limit all nonlinear ξ terms are discarded, thus yielding a dispersion relation for the wave spectrum:

$$\frac{1}{\tau} = -\frac{h^3}{3\eta} \left[\gamma q^4 + \frac{\partial p_{el}}{\partial h} q^2 \right] \quad (4)$$

The exponentially fastest-growing mode given by the maximum of Equation (4) eventually dominates the mode spectrum. It has the wavelength $\lambda = 2\pi/q_{max}$:

$$\frac{\lambda}{\lambda_0} = \left(\frac{E_p}{E_0} \right)^{-\frac{3}{2}} \quad (5)$$

with

$$\frac{\tau}{\tau_0} = \left(\frac{E_p}{E_0} \right)^6 = \left(\frac{\lambda}{\lambda_0} \right)^4 \quad (6)$$

where the following reduced quantities were introduced:

$$q_0 = \frac{\gamma}{\varepsilon_0 \varepsilon_p (\varepsilon_p - 1)^2 U^2} \quad (7a)$$

$$\lambda_0 = \frac{2\pi}{q_0} \quad (7b)$$

$$E_0 = q_0 U \quad (7c)$$

$$\tau_0 = \frac{3\eta}{\gamma h_0^3 q_0^4} \quad (7d)$$

These equations reveal an interesting property of the EHD instability: the variation of the characteristic time constant with the electric field is four orders of magnitude higher than the variation of λ with the electric field. This has the important consequence that very small lateral variations of the electric field (e.g., introduced by a slight variation in the plate spacing d) have a significant effect on the onset of the instability, while their effect on λ may be negligible. Even for a carefully designed

experimental configuration, the instability does not typically develop everywhere in the capacitor at the same time. Instead, an instability front sweeps laterally across the sample. This property is exploited in our study to monitor the development and completion of the instability in low-viscosity materials.

To compare the destabilization of materials with differing viscosities, it is useful to introduce an additional set of scaling relations. The inverse of the time constant defines a rate for the lateral displacement of material over a distance λ . Multiplied by η this defines a characteristic shear stress:

$$\sigma = \frac{\eta}{\tau} \quad (8)$$

Defining

$$\sigma_0 = \frac{\eta}{\tau_0} \quad (9)$$

introduces the further scaling equation

$$\frac{\sigma}{\sigma_0} = \left(\frac{E_p}{E_0} \right)^6 \quad (10)$$

3. Results and Discussion

To demonstrate the suitability of low-viscosity polymers, pattern formation and replication were studied first. Approximately 100-nm-thick resist layers were spin-cast onto silicon wafers, which were opposed by a second silicon wafer to leave an air gap. The details of device assembly and characterization are given in the Experimental Section. The materials utilized are summarized in Table 1. Two device geometries were employed as previously described: capacitors with either planar or structured top electrodes. The use of an unstructured top electrode resulted in the formation of a locally hexagonal array of columns (Figure 2). For all the studied materials, the instability proceeded in the same fashion: the initial amplification of a low-amplitude capillary wave in Figure 2A resulted in an array of columns spanning the two electrodes in Figure 2C. The initially observed wavelength in Figure 2A of 2.5 μm as well as the final intercolumn spacing are in good agreement with the stability analysis outlined in the previous section. Despite the much shorter destabilization time of ~ 7 s, the pattern formation process of Figure 1 is reminiscent of the well-studied case of generic polymers,^[17–19] thus confirming the same underlying physical mechanism. Figure 2B is an intermediate snapshot revealing the pattern formation kinetics.

While the pattern on the left-hand side of the image is reminiscent of the early-stage instability of Figure 2A, full column formation is seen on the right-hand side of the image. The origin of this lies in the small lateral variation of the capacitor plate spacing d (by a few $\mu\text{m cm}^{-1}$). Because of the scaling of τ with the sixth power of the electric field [Eq. (5)], this results in an instability wave propagating from the right-hand part of the sample (small d) to the left. The much lower dependence of the wavelength on the electric field of Equation (4), on the other hand, explains the fact that the lateral variation of the final pattern (Figure 2C) is only very small.

The use of a patterned top electrode gives rise to a laterally varying electric field. For air-gap widths larger than the film thickness and for high pattern densities on the opposing electrode, the initial phase of the instability is similar to the case of Figure 2A.^[20] Figure 3A–D shows the evolution of pattern formation following this initial stage. Starting from an initial homogeneous undulation, the wave pattern couples to the lateral field variation, and the further growth of the instability is focused in the direction of the highest electric field and is thereby guided towards the protruding patterns of the top mask. This gives rise to a pillar pattern spanning the substrate and the top electrode at locations of smallest interelectrode spacing (Figure 3A), which by coalescence (Figure 3B,C) eventually forms a positive replica of the master electrode (Figure 3D). Different from the case shown in Figure 2, the coalescence of the capillary plugs bridging the substrates and the protruding parts of the top electrode proceeds rapidly, and forms an integral part of the pattern replication kinetics. As shown before,^[20] the seamless sequence of capillary instability followed by the coalescence of the initial capillary bridges gives rise to the near-perfect replication of a master pattern, which is quite robust with respect to the size and periodicity of the mask and is not visibly influenced by the small overall wedge geometry of the capacitor (see Figure 3D–H). Once the correct sample parameters are identified, high-fidelity pattern replication over the entire electrode area ($100 \times 100 \mu\text{m}^2$ in our case) can be obtained. The patterning time does not depend on sample size and is limited only by the ability to create a capacitor geometry with sufficient precision in interplate spacing. Again, the advantage of using a low-viscosity polymer is the completion of the entire process in less than 10 s.

The relatively high speed of the EHD process sets a strict time limit for the termination of the pattern formation process, since too long exposure of the liquefied film to the electric field may lead to undesired coarsening of the pattern by coalescence. A convenient way to follow the progress of pattern formation and replication involves monitoring the current across the

Table 1. Parameters of the polymer materials.

	Material	Chemical structure	η [Pa s]	T_g [°C]	γ [mN m ⁻¹]	ϵ_p
EC	ethyl cellulose	[C ₆ H ₇ O ₂ (OC ₂ H ₅) ₃] _n	0.084	100–130	28.5	3.5
PVA	poly(vinyl alcohol)	(C ₂ H ₄ O) _n	0.073	85	50	2
PVAc	poly(vinyl acetate)	(C ₄ H–6O ₂) _n	0.225	25–30	57.4	5.8
PVP	poly(vinyl pyrrolidone)	(C ₆ H ₉ NO) _n	1.032	110	56	2.3
PCL-diol	polycaprolactone	(C ₁₀ H ₁₉ O ₅) _n	0.557	45	49	2

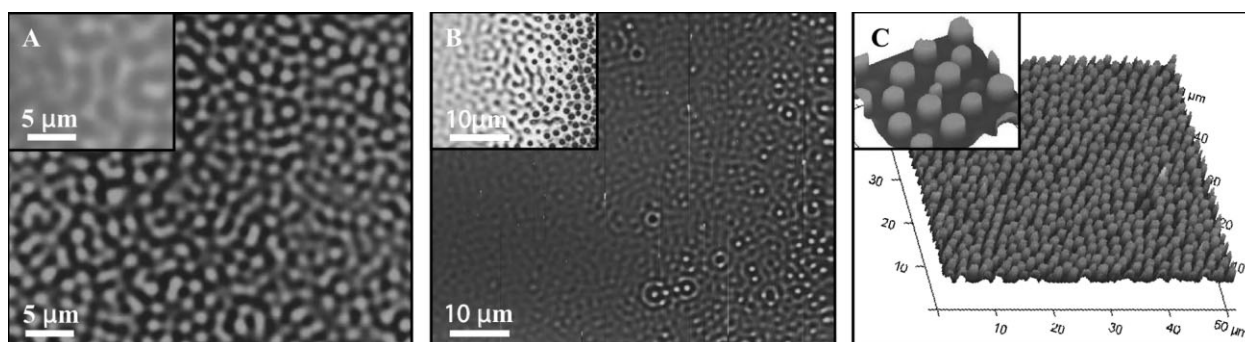


Figure 2. Atomic force microscopy (AFM) images of the instability evolution of a 100-nm-thick PVAc film in a homogeneous electric field. A) Initial surface undulation after 7.0 ± 4 s, which evolves into columns 250 ± 17 nm in height with a diameter of ~ 2 μm and an average intercolumn spacing of 2.5 ± 0.5 μm in (C). B) The intermediate stage (inset: optical image) shows the consequence of a slight variation in the interplate spacing, which indicates a range of stages of the instability (left: undulations; right: columns). While the lateral variation of the electric field has a strong effect on the destabilization kinetics, its effect on the pattern that evolves is negligible (see text).

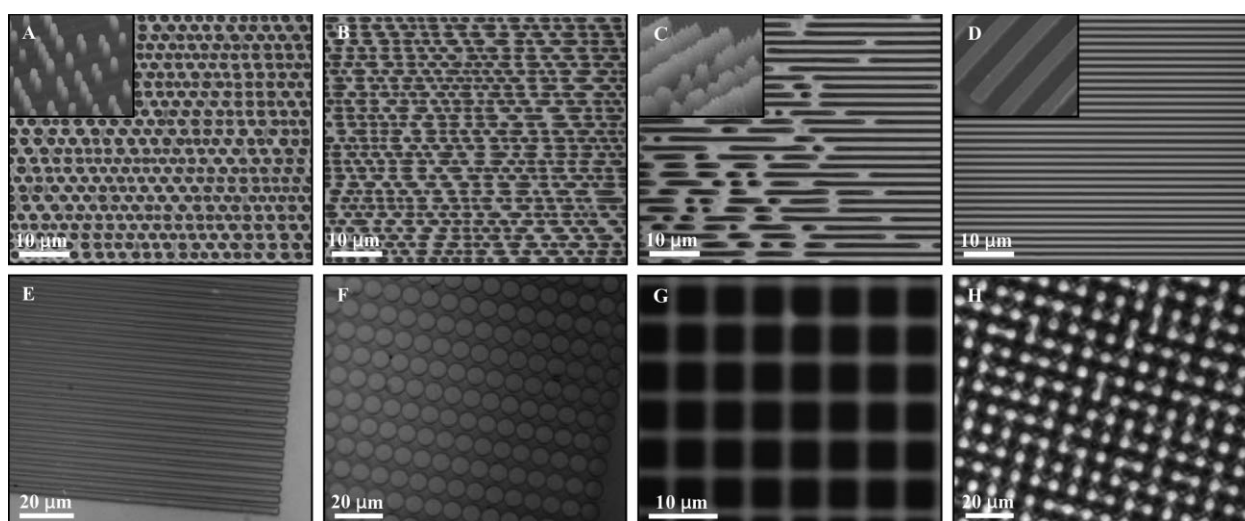


Figure 3. Optical images of pattern formation in EC films in laterally heterogeneous electric fields. A–D) Pattern replication of a line grating, imaged after immobilization of the thin film and removal of the master electrode. An overall wedge geometry allowed different stages of the pattern replication process to be captured ($h = 100$ nm, $U = 40$ V, d decreasing from left to right). A) Initial capillary plugs spanning the substrate and protruding lines; B, C) increasing coalescence of the capillary plugs; and D) final replicated grating. Corresponding AFM images are shown in the insets. E–H) High-fidelity EHD replication in EC films showing the robustness of pattern replication with respect to the parameters of the electrode.

sample. Most dielectric organic resists have a short-circuit current in their liquid state, mostly mediated by ionic impurities in the materials.^[2] For 100-nm-thick films (see Experimental Section), this current is on the order of 10 mA cm^{-2} . For the patterned materials in this study, the time evolution of the current can be subdivided into three regimes: an initial current of several mA cm^{-2} , an intermediate regime during which the current increases, and a final plateau of $\sim 10 \text{ mA cm}^{-2}$.

In situ optical investigation with a transparent electrode was used to correlate the structure formation process with the measured current. Current traces correlated with the evolving EHD topography are shown in Figure 4. The initial current corresponds to the sample before pattern formation sets in, mediated by the spacer particles. The onset time of the current rise t_i coincides with the time when the first columns bridge the two plates at the location of smallest plate spacing (right-hand side of Figure 2B). Because of the exponential variation of the

local film thickness with time [Eq. (3)], t_i can be approximated by the characteristic time τ of Equation (5) for this plate spacing. As the instability front sweeps across the sample, the number of capillary plugs increases, thereby increasing the short-circuit current. The current saturates ($t = t_f$) once the entire sample is covered by capillary bridges, which is comparable to the value of τ for the largest value of d of the sample. For the sample consisting of two planar electrodes, pattern coarsening does not lead to a further current increase, because the integral cross-sectional area of the capillary plugs does not increase.

The interpretation of the current increase in the case of pattern replication is slightly more complex. While the same basic principle of the initial pattern-forming process of the previous paragraph also applies here, the initial columns are localized at lateral positions where the top electrode protrudes downwards to the film (Figure 3A). These columns are laterally

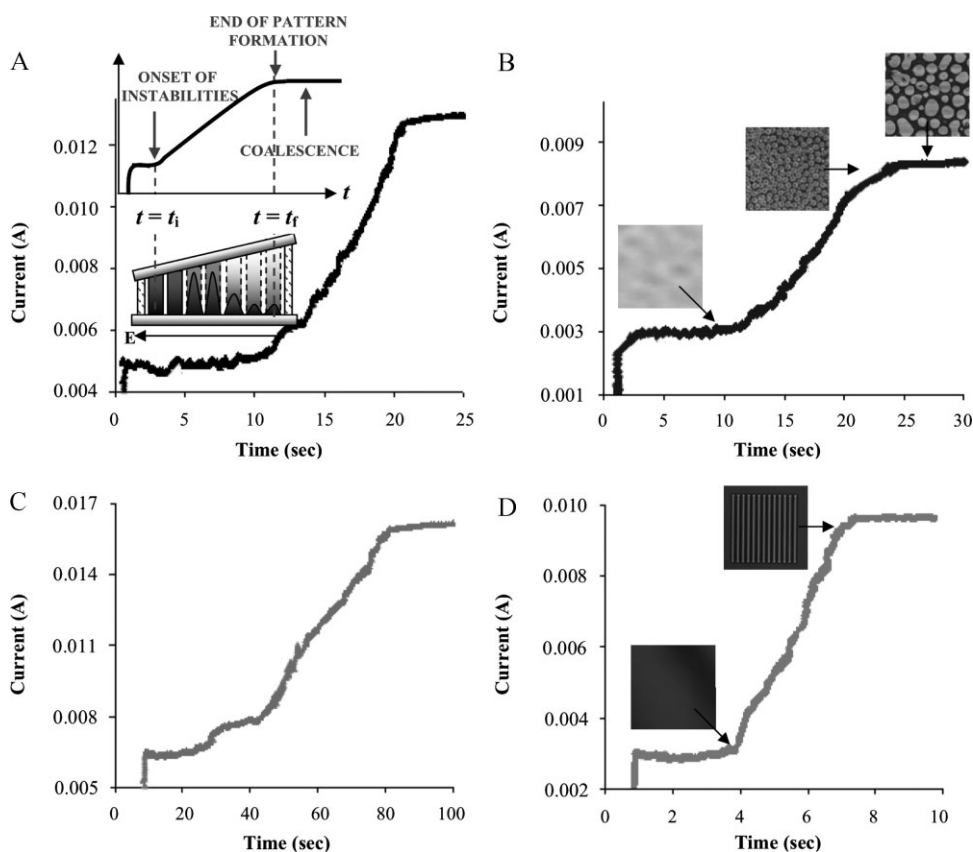


Figure 4. Short-circuit current across capacitor devices as a function of time during the EHD patterning process. A–C) Plots for PVA, PVAc, and PVP films in a homogeneous electric field with viscosities of 0.073, 0.225, and 1.032 Pa s, respectively. Inset in (A): Schematic representation of a typical S curve for current flow through the capacitor device during patterning, which indicates the onset and termination of the experiment. Insets in (B): Optically observed patterns during the initial and intermediate stages of pattern formation and AFM image of the late stage of the process, where coalescence has coarsened the initial pattern (indicated by arrows). C) Schematic representation of an exaggerated wedge geometry, which demonstrates the correspondence between pattern evolution and current curves as a function of the plate spacing. D) EC with $\eta = 0.084$ Pa s in a laterally varying electric field caused by a topographic grating. The insets show optical images of the sample at the various stages. The parameters of all measurements were $h \approx 100$ nm, $d \approx 250$ nm (average), $U = 40$ V, and $T = 135$ °C.

connected to unpatterned parts of the film at locations of lower electric field.^[20] With time more material is drawn into the columns at high-electric-field locations, thus leading to an increase in their diameter, to their coalescence (Figure 3B,C), and eventually to the replication of the electrode structure (Figure 3D). The current increase is therefore a convolution of the instability front that laterally sweeps across the sample with this coarsening process. While t_i is comparable with τ for the location of smallest d of the sample, t_f signifies the time when the entire pattern replication process is terminated. The characteristic current trace of a sample with a patterned top electrode is shown in Figure 4D.

Figure 5A shows the variation of the film destabilization time with the viscosity of the polymer. To compare samples with different experimental parameters, the data are plotted as a function of η/σ , where all other experimental parameters are absorbed in the shear stress σ . While the optically detected onset of the instability and the onset of the current increase t_i are well described by the prediction of Equation (9), the completion of patterning t_f is offset towards higher values compared to the prediction of τ , thus indicating that the

completion of patterning systematically exceeds the longest time constant of the system.

As qualitatively extracted from Figure 2, the marked temporal evolution of the instability caused by small inhomogeneities in the electric field has only a minor influence on the structural parameters of the instability (i.e., λ). This is quantitatively shown in Figure 5B. For a PVAc film, λ changed by only 12% over a lateral distance of 45 μ m, despite a relative variation of the time constant by a factor of 2.5. This is a consequence of the power-law relations of Equations (4) and (5), with τ and λ differing in their response to variation in the electric field by four orders of magnitude.

Finally, we address the question of how far the small but finite current across the device violates the assumption of the linear stability analysis that models the polymer layer as a perfect dielectric. A finite polymer conductivity lowers the electric field in the layer and increases the electrostatic stress at the surface, as predicted in the leaky dielectric model by Pease and Russel.^[3,14,15] While this marginally alters λ , its effect on the value of τ may be significant (again, because of the higher-order scaling of τ with the electrostatic surface pressure). The fact that

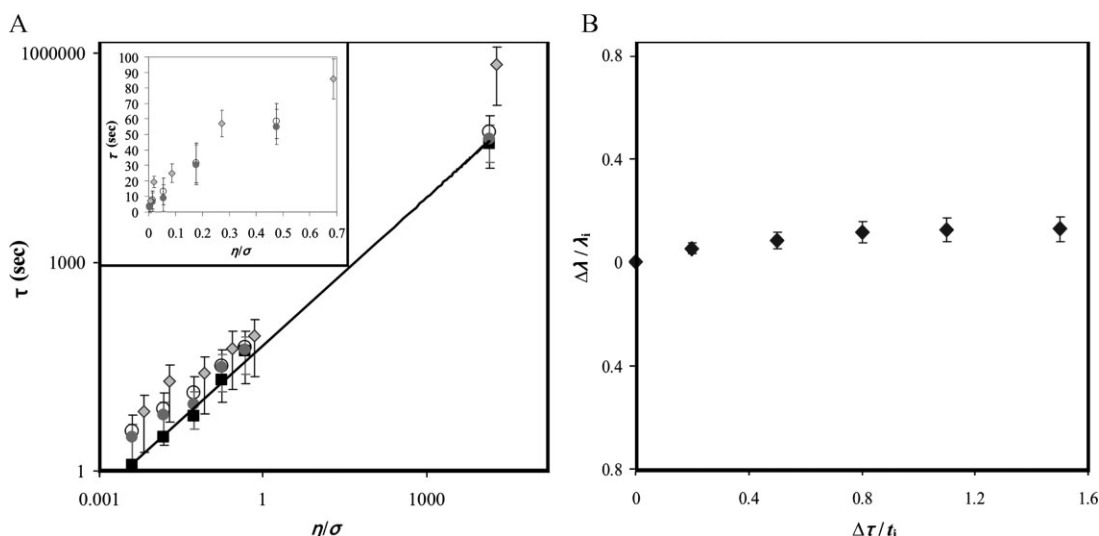


Figure 5. A) Variation of the instability time constant τ with viscosity η in terms of Equation (9). The data obtained by current monitoring (filled circles: $\tau = t_i$) and optically determined values of τ (open circles) agree within their error margins and are well described by the prediction of Equation (9) (line). The data obtained from the termination times (diamonds, $\tau = t_f$) follow the same trend, but are offset towards longer times. Inset: Details of the initial 100 s. B) Variation of pattern periodicity $\Delta\lambda/\lambda_i = (\lambda - \lambda_i)/\lambda_i$ as a function of the variation of the patterning time $\Delta\tau/t_i = (\tau - t_i)/t_i$ for a PVAc film ($\lambda_i = \lambda(t_i)$). Over a lateral distance of 45 μm , the wavelength changed only by 12% compared to a variation of $\Delta\tau/t_i$ by a factor of 2.5.

the time constants in Figure 5 are well described by a model that neglects the finite conductivity suggests the suitability of the simpler model used in our data analysis.

4. Conclusions

In summary, we have explored the use of low-viscosity materials for fast EHD patterning. Different from the typically published polymers, the studied materials not only have a thermally accessible glass transition temperature but also exhibit very low viscosities upon softening. This enables the completion of the EHD process within seconds rather than hours, thus increasing the technological appeal of this technique. The rapid pace of the EHD instability demonstrated in these experiments requires, however, an improved monitoring method of the patterning process. We have therefore exploited the small but finite current that flows through the device during pattern formation. The current trace has a sigmoidal shape that defines the characteristic onset and completion time of the EHD process. While t_i corresponds closely to the characteristic time of the instability τ , t_f is primarily of practical interest, by indicating the completion of pattern formation and replication. From a practical point of view, it is essential that the sample is solidified at $t \approx t_f$ to prevent a deterioration of the pattern by coarsening. Because of the quick patterning time, rapid sample quenching is important, possibly requiring a sample support that allows in situ cooling. Importantly, our study shows that, despite the much shorter patterning times, the EHD process is similar to that of high-viscosity polymers and is therefore well described by a linear stability analysis.

This technique should be readily extendable to feature sizes down to 10 nm. Reduction of, for example, the interfacial surface tension further accelerates pattern replication and

reduces the characteristic pattern size. In the lithographic mode, electrostatically induced structure formation is not limited to the intrinsic wavelength, which allows the replication of a large range of feature sizes for otherwise identical experimental parameters. Reducing the replicated feature size further decreases the time constant to a millisecond and below. In this accelerated mode, EHL is a promising prospect for the rapid, straightforward, and low-cost replication of submicrometer patterns.

5. Experimental Section

Materials: All resists (listed in Table 1) were purchased from Sigma–Aldrich, except for ethyl cellulose (Fluka), and were used without further purification. Polystyrene ($M_w = 100 \text{ kg mol}^{-1}$, $M_w/M_n < 1.07$) was purchased from Polymer Standards Service GmbH, Mainz, Germany. Toluene, chloroform, acetone, and isopropanol were purchased from Fisher Scientific. Highly polished p-doped silicon wafers, with $\langle 100 \rangle$ crystal orientation (Wafernet GmbH, Eching, Germany) were used as substrates. Electron-beam-patterned silicon structures were obtained from X-lith eXtreme Lithography, Ulm, Germany. Indium tin oxide (ITO)-coated glass slides with a resistance of $112 \Omega \text{ cm}^2$ were used as transparent substrates for in situ optical observations.

Experimental procedure: Thin films with an initial thickness of $h = 100 \pm 20 \text{ nm}$ were spin-cast onto 1 cm^2 silicon substrates from toluene or chloroform solutions with typical concentrations of 2–3% polymer by weight. Prior to spin-coating, the substrates were cleaned in a “piranha” solution consisting of 98% H_2SO_4 /30% H_2O_2 (3:1), followed by thorough rinsing with deionized water and drying under nitrogen. The ITO-coated glass slides were cleaned

by scrubbing in soap water at 75 °C and washing in an ultrasonic bath with acetone and isopropanol, followed by irradiation for 20–30 min in a UV–ozone cleaner. Immediately before device assembly, all substrates and electrodes were subjected to snow-jet cleaning. Capacitor devices were assembled using a film-covered substrate as lower electrode. Facing it, planar or topographically structured silicon wafers were mounted leaving a thin air gap. The overall electrode spacing d was adjusted by using silicon oxide colloids as spacers. A slight misalignment of the two electrodes resulted in a slight wedge geometry, which led to a variation of d from ~ 100 nm to ~ 1 μ m across the entire sample width of 1 cm. Both electrodes were electrically contacted using silver paint (Electrodag 1415M).

The films were liquefied by thermal annealing: the temperature was raised above the T_g of the resist, and a voltage of 40 V was applied to the capacitor device. The experiment was terminated by quenching the assembly to room temperature before removing the electric field. Current curves were recorded during each EHD patterning process. A sparse distribution of sample imperfections and the fact that the silica colloids were wetted by the polymer gave rise to a small current prior to film patterning. Time $t = 0$ marks the time that the voltage is applied to the capacitor. The slight offset in current recording arose from a delay in current recording.

After each experiment, the top electrode was removed and the formed pattern was analyzed by optical microscopy, atomic force microscopy (AFM), and scanning electron microscopy (SEM).

Characterization: The evolving patterns were observed via in situ imaging using an inverted optical microscope (Olympus GX 51). The smallest visually detectable amplitude fluctuation in the film (~ 5 nm) determined the onset of pattern formation. NanoScope IV Multimode and Dimension 3100 (Digital Instruments, Santa Barbara, CA) atomic force microscopes were employed to quantitatively determine the sample topography. All the measurements were performed in air under ambient conditions using the tapping mode. NSG 20 cantilevers with a resonance frequency of 260 kHz and a stiffness of 28 N m^{-1} were used. Height and phase images were analyzed with the Nanoscope software (Digital Instruments). The AFM measurements yielded the film thickness h , the plate spacing d , the characteristic wavelength λ , and the width and height of the replicated patterns. SEM was used to support the AFM measurements. A LEO ULTRA 55 SEM instrument including a Schottky emitter (ZrO/W cathode) with an acceleration voltage of 10.0 kV was used. The polymer viscosities were measured using a 1° cone and plate rheometer (Physica MCR 501, Anton Pear) at room temperature. A constant-

voltage source was used to apply a voltage of 40 ± 1 V across the capacitor devices and the resulting current was measured using a Keithley Model 2000 multimeter.

Acknowledgements

This work was funded by Kodak European Research, Cambridge.

- [1] E. Schaffer, T. Thurn-Albrecht, T. P. Russell, U. Steiner, *Nature* **2000**, *403*, 874–877.
- [2] E. Schaffer, T. Thurn-Albrecht, T. P. Russell, U. Steiner, *Europhys. Lett.* **2001**, *53*, 518–524.
- [3] N. Wu, W. B. Russel, *Nano Today* **2009**, *4*, 180–192.
- [4] J. W. Swan, *Proc. R. Soc. London* **1897**, *62*, 38–46.
- [5] L. Tonks, *Phys. Rev.* **1935**, *48*, 562–568.
- [6] J. Frenkel, *Phys. Z. Sowjetunion* **1935**, *8*, 675–679.
- [7] J. Heier, J. Groenewold, U. Steiner, *Soft Matter* **2009**, *5*, 3997–4005.
- [8] N. E. Voicu, S. Ludwigs, U. Steiner, *Adv. Mater.* **2008**, *20*, 3022–3027.
- [9] K. Leach, Z. Lin, T. Russell, *Macromolecules* **2005**, *38*, 4868–4873.
- [10] M. Dickey, E. Collister, A. Raines, P. Tsiartas, T. Holcombe, S. Sreenivasan, R. Bonnacaze, C. Willson, *Chem. Mater.* **2006**, *18*, 2043–2049.
- [11] J. R. Melcher, *Field-Coupled Surface Waves*, MIT Press, Cambridge, MA, **1963**.
- [12] A. Vrij, *Discuss. Faraday Soc.* **1966**, *42*, 23.
- [13] F. B. Wyart, P. Martin, C. Redon, *Langmuir* **1993**, *9*, 3682–3690.
- [14] L. F. Pease, W. B. Russel, *J. Chem. Phys.* **2003**, *118*, 3790–3803.
- [15] L. F. Pease, W. B. Russel, *Langmuir* **2004**, *20*, 795–804.
- [16] A. Oron, S. H. Davis, S. G. Bankoff, *Rev. Mod. Phys.* **1997**, *69*, 931–980.
- [17] S. Harkema, PhD Thesis, University of Groningen, 2006, <http://irs.ub.rug.nl/ppn/291147801>.
- [18] S. Harkema, U. Steiner, *Adv. Funct. Mater.* **2005**, *15*, 2016–2020.
- [19] M. D. Morariu, N. E. Voicu, E. Schaffer, Z. Q. Lin, T. P. Russell, U. Steiner, *Nat. Mater.* **2003**, *2*, 48–52.
- [20] N. E. Voicu, S. Harkema, U. Steiner, *Adv. Funct. Mater.* **2006**, *16*, 926–934.

Received: January 15, 2010

Revised: March 24, 2010

Published online: May 19, 2010